Tuning the Electrical Memory Characteristics from Volatile to Nonvolatile by Perylene Imide Composition in Random Copolyimides

ARTICLE *in* MACROMOLECULES · MAY 2012

Impact Factor: 5.8 · DOI: 10.1021/ma300732m

6 AUTHORS, INCLUDING:

Yi-Cang Lai
National Taiwan University
8 PUBLICATIONS **210** CITATIONS
SEE PROFILE

Tomoya Higashihara
Yamagata University
198 PUBLICATIONS **3,183** CITATIONS
SEE PROFILE

Mitsuru Ueda
Kanagawa University
655 PUBLICATIONS **9,854** CITATIONS
SEE PROFILE

Wen-Chang Chen
National Taiwan University
274 PUBLICATIONS **6,906** CITATIONS
SEE PROFILE

Macromolecules

Article

pubs.acs.org/Macromolecules

Tuning the Electrical Memory Characteristics from Volatile to Nonvolatile by Perylene Imide Composition in Random Copolyimides

Tadanori Kurosawa,[†,⊥] Yi-Cang Lai,[‡,⊥] Tomoya Higashihara,[†] Mitsuru Ueda,*[,†] Cheng-Liang Liu,*[,§,#] and Wen-Chang Chen*[,‡,∥]

[†]Department of Organic and Polymeric Materials, Tokyo Institute of Technology, 2-12-1 Ookayama, Meguro-ku, Tokyo 152-8552, Japan

[‡]Institute of Polymer Science and Engineering, National Taiwan University, Taipei 10617, Taiwan

[§]Department of Organic Device Engineering and Research Center for Organic Electronics, Yamagata University, Yonezawa, Yamagata 992-8510, Japan

[∥]Department of Chemical Engineering, National Taiwan University, Taipei 10617, Taiwan

Supporting Information

ABSTRACT: Random copolyimides, **PI−PBIX**, with different compositions of 4,4′-(hexafluoroisopropylidene)diphthalic anhydride (**6FDA**), *N*,*N*′-bis(4-aminophenyl)-3,4,9,10-perylenebis(dicarboximide) (**PBI**), and 4,4′-diamino-4″-methyltriphenylamine (**AMTPA**) were designed and synthesized for resistive-switching memory device applications. By varying the feeding ratio of monomers, **PI−PBIX** (where **X** = 0, 1, 2.5, 5, and 10 for molar composition of repeating units containing **PBI**) showed tunable optical and electronic properties through the charge transfer between **AMTPA** and **PBI**. Also, the memory devices prepared from **PI−PBIX** sandwiched between ITO and Al electrodes exhibited the tunable electrical bistability from the volatile to nonvolatile write once read many-times (WORM) memory characteristics as the **PBI** composition increased. The OFF/ON electrical switching transition was mainly attributed to the charge-transfer mechanism for charge-separated high conductance, based on the analysis of density function theory. Also, the volatility of **PI−PBIX** device depended on the stability of charge-transfer complex and charge trapping sites. The deep LUMO energy level of the **PBI** moiety increased the back-charge-transfer energy barrier and prevented recombination of segregated charges even through applying the high negative and positive voltage. The study revealed that the memory characteristics could be tailored from the donor−acceptor composition in the random copolyimides.

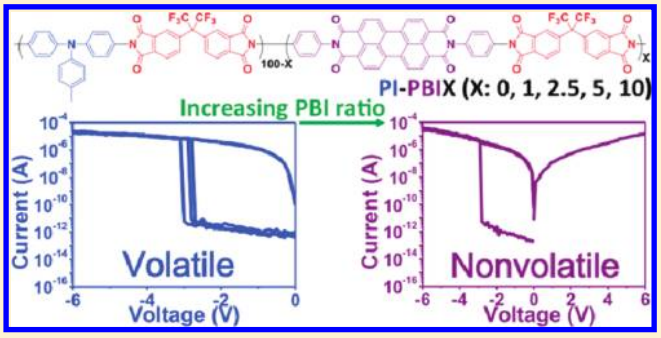

INTRODUCTION

Over the past few decades, tremendous efforts have been made on the investigation of resistive switching memory for the growing demand of next-generation information and communication technology with high speed, low operation voltage and high packing density.[1−9] The resistive switching phenomena are based on the electrically voltage-stimulated change in a current response composed of a metal/insulating or semiconducting materials/metal memory cells. A low-conductivity state (OFF) is switched by a threshold voltage to a high-conductivity state (ON). Most of these simple stacking memory devices obtained more powerful functionalities using metal oxides as active memory layers.[1,2] On the other hand, resistive memory devices based on organic or polymeric materials have been recognized as one of emerging data storage media, especially targeting for flexible electronics and molecular design guide on chemical structures.[3−9]

Polymeric materials that exhibited the resistive switching characteristics included functional polyimides (PIs),[10−20] conjugated polymers,[21,22] polymers with specific pendent chromophores,[23−25] and polymer nanocomposites (metal nanoparticles (NPs),[26,27] fullerene,[28,29] and graphene oxide (GO)[30,31] embedded). Recently, significant research activities have existed on functional PIs for electrical memory devices due to their advantages such as excellent thermal and oxidative stability, chemical resistance, mechanical strength, electrical properties, and rich structural design.[10−19] Functional PIs containing both electron-donating and electron-withdrawing groups contributed to the electronic transition based on electric-field-induced charge-transfer complex[10−13,17−20] or

Received: April 9, 2012
Revised: May 14, 2012
Published: May 29, 2012

Scheme 1. Synthesis of the Studied PI−PBIX Copolyimides

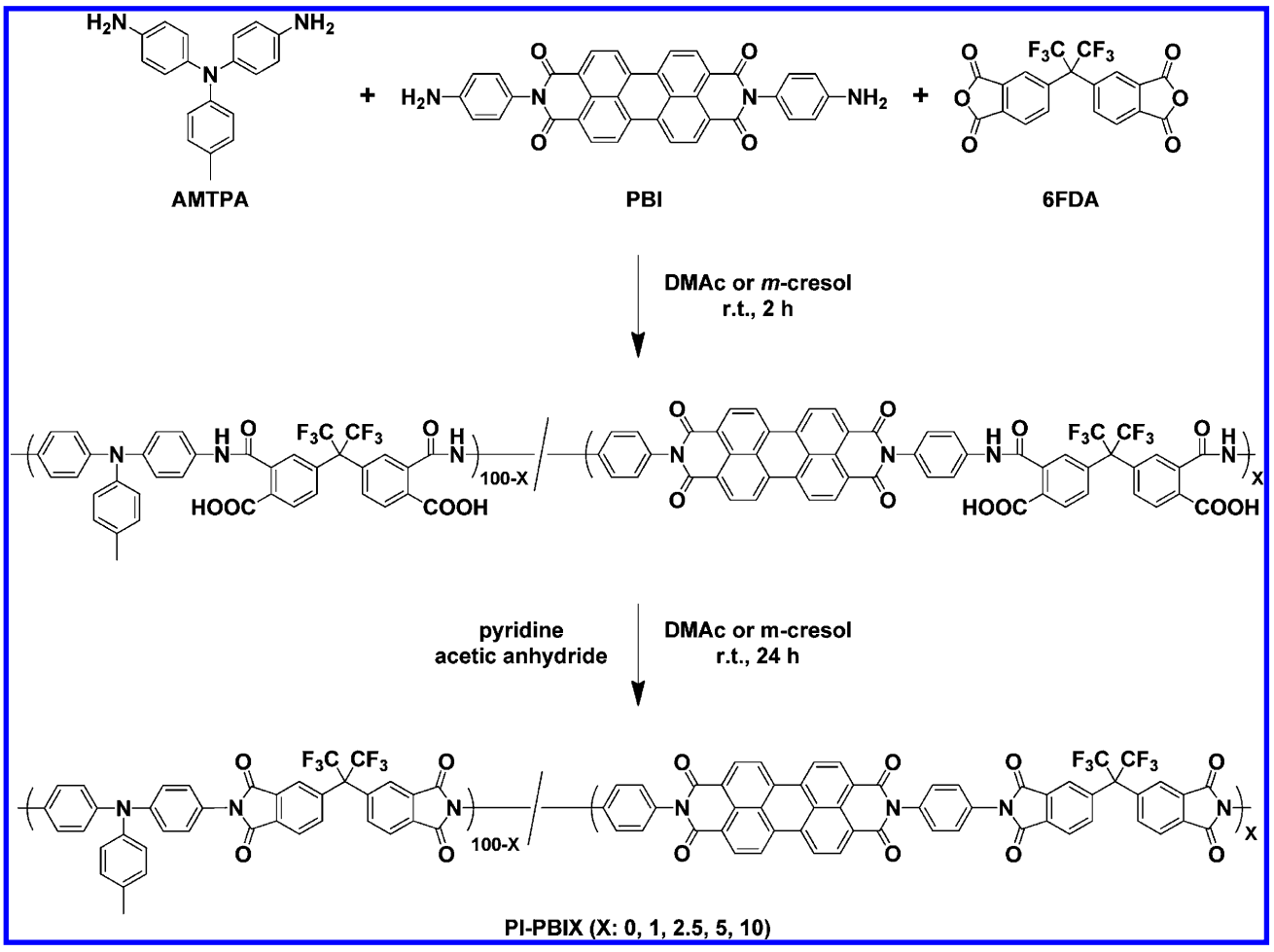

charge trapping environment,[14−16] which determined the volatility of the memory device. Specifically, **TP6F−PI**, electron-donating triphenylamine (TPA) attached with electron-accepting phthalimide, exhibited dynamic random access memory (DRAM) behavior[10] while **PYTPA−PI** (consisting of TPA-substituted diphenylpyridine and phthalimide) showed improved DRAM performance[11] as reported by Kang and coworkers. Also, the same group reported both **OXTA-PIa**[12] and **AZTA-PIa**[13] containing **TPA** substituted with 1,3,4-oxadizaole and triazole moieties, respectively, which showed nonvolatile write once read many-times (WORM) memory characteristics. Meanwhile, Ree et al. proposed **6F-2TPA PI** for stable digital nonvolatile WORM and volatile DRAM characteristics depending on film thickness.[14] A flash-type memory of **F-HAB-TPAIE PI**[15] bearing two pendent **TPA** groups and a unipolar WORM memory of **6F-HTPA PI**[16] with an attached hydroxyl group on the **TPA** groups were reported. Our group also found that the mono- or dual-mediated phenoxy linkages between the **TPA** and phthalimide moieties significantly influenced the volatile behavior.[17] Although a number of PIs showing various memory properties have been reported as have been described above, the relationship between the PIs structure and its memory characteristics still remains unclear. Particularly, clarifying the effect of PIs structure on the volatility is a subject of utmost importance in the development of polymer memory devices. Therefore, it would be significant to give a guideline for controlling the volatility through the design of PIs structure.

On the other hand, a variety of perylenedisimide derivatives have been synthesized and studied due to their outstanding n-type semiconducting properties originating from the large conjugation and high electron affinity of the core perylenebisimide unit.[36] When perylenebisimide is introduced as an electron acceptor in the donor−acceptor polymers, such distinctive natures of perylenebisimide are effective to the stabilization of radical anion induced by charge transfer (CT) from donor to acceptor, resulting in a stable CT state. As for memory properties, the key factor to determine the volatility is the stability of the CT state. If it is unstable, the resulting memory characteristic would be a volatile one and vice versa. Therefore, introducing perylenebisimide in the polymer structure could induce nonvolatile memory. Also, it might be possible to control the volatility by changing the content of perylenebisimide.

In this paper, functional random copolyimides (coPIs) (**PI−PBIX**; where **X** is the molar content of the repeating unit consisting of *N*,*N*′-bis(4-aminophenyl)-3,4,9,10-perylenebis(dicarboximide) (**PBI**) and 4,4′-(hexafluoroisopropylidene)diphthalic anhydride (**6FDA**)) based on 4,4′-diamino-4″-methyltriphenylamine (**AMTPA**), **PBI**, and **6FDA** were synthesized (Scheme 1). They were designed for the purpose of controlling the volatility and revealing nonvolatile memory characteristics by introducing the varied ratio of **PBI** comonomer. Thermal, optical, and electrochemical properties of the new synthesized coPIs were characterized. The memory behaviors of **PI−PBIX** were conducted by a simple sandwich

dx.doi.org/10.1021/ma300732m | *Macromolecules* 2012, 45, 4556−4563

device configuration of spin-coated PIs film between ITO and Al electrode. Changing the feeding ratio of **PBI** comonomer was effective for the redistribution of electronic structures, resulting in different memory switching behaviors. Comparative study on the switching behavior and mechanism of **PI−PBIX** are also reported including the electrical analysis and investigation on structural dependence. These results were expected to provide the new strategy to design PIs-based memory device applications.

EXPERIMENTAL SECTION

Materials. The materials were used without further purification unless otherwise noted. Dehydrated *N*,*N*-dimethylacetamide (DMAc), dehydrated pyridine, and acetic anhydride were purchased from Wako Pure Chemical Industries, Ltd. (Japan). *m*-Cresol was purchased from Kanto Chemical Co., Inc. (Japan). **6FDA** was purchased from TCI (Japan) and purified by sublimation. **PBI** was synthesized according to the previous report.[32] **AMTPA** was kindly donated by JSR Corp. (Japan).

Polymer Synthesis. *Poly[4,4′-diamino-4″-methyltriphenylamine−hexafluoroisopropylidenediphthalimide] (**PI−PBI0**).* To a solution of **AMTPA** (0.289 g, 1.00 mmol) in DMAc (5.00 mL) was added **6FDA** (0.444 g, 1.00 mmol) under nitrogen. The mixture was stirred for 2 h at room temperature to give a viscous poly(amic acid) (PAA) solution. Excess amounts of acetic anhydride (1.50 mL) and pyridine (1.50 mL) were then added to the above PAA solution and stirred for 24 h. The resulting solution was poured into methanol, and the precipitate was collected by filtration. The final product was washed with methanol and dried at 200 °C for 5 h under vacuum to yield 0.666 g (95%). The number-average molecular weight (M_n) and weight-average molecular weight (M_w) estimated from size exclusion chromatography (SEC) were 4.25×10^4 and 11.2×10^4, respectively, with the polydispersity index (PDI = M_w/M_n) of 2.64. IR (KBr), ν (cm^{-1}): 1782, 1720 (C═O stretching), 1377 (C−N stretching). ^{1}H NMR (DMSO-d_6, δ, ppm): 8.13 (d, J = 7.8 Hz, ArH, 2H), 7.94 (d, J = 7.8 Hz, ArH, 2H), 7.79 (s, ArH, 2H), 7.36 (d, J = 9.0 Hz, ArH, 4H), 7.21 (d, J = 8.7 Hz, ArH, 2H), 7.15−7.08 (m, ArH, 6H), 2.30 (s, $ArCH_3$, 3H). Anal. Calcd for $C_{38}H_{21}N_3$: C, 65.4; H, 3.03; N, 6.02. Found: C, 64.9; H, 3.21; N, 6.17.

*Poly[4,4′-diamino-4″-methyltriphenylamine−hexafluoroisopropylidenediphthalimide-co-N,N′-bis(4-aminophenyl)-3,4,9,10-perylenebis(dicarboximide)−hexafluoroisopropylidenediphthalimide] (**PI−PBIX**).* **6FDA** (0.444 g, 1.00 mmol) was added to a solution of **AMTPA** and **PBI** in *m*-cresol (5.00 mL), and the mixture was stirred for 2 h at room temperature to afford a viscous solution. The total amount of **AMTPA** and **PBI** was set to 1.00 mmol. The molar ratios of **PBI** to **AMTPA** were set to be 1, 2.5, 5, and 10 mol % for **PI−PBI1**, **PI−PBI2.5**, **PI−PBI5**, and **PI−PBI10**, respectively. A reaction mixture of acetic anhydride (1.50 mL) and pyridine (1.50 mL) was added to the above PAA solution. The reaction mixture was stirred at room temperature under a nitrogen atmosphere for 24 h. The resulting solution was poured into methanol, and the precipitate was collected by filtration and washed with methanol. The product was finally dried at 200 °C for 5 h under vacuum. **PI−PBI1**, **PI−PBI2.5**, **PI−PBI5**, and **PI−PBI10** were obtained in the yields of 85, 84, 81, and 92%, respectively. IR (KBr) of **PI−PBI1**, ν (cm^{-1}): 1786, 1724 (C═O stretching of phthalimide), 1662 (C═O stretching of PBI unit), 1381 (C−N stretching). IR (KBr) of **PI−PBI2.5**, ν (cm^{-1}): 1786, 1724 (C═O stretching of phthalimide), 1662 (C═O stretching of PBI unit), 1381 (C−N stretching). IR (KBr) of **PI−PBI5**, ν (cm^{-1}): 1786, 1724 (C═O stretching of phthalimide), 1658 (C═O stretching of PBI unit), 1377 (C−N stretching). IR (KBr) of **PI−PBI10**, ν (cm^{-1}): 1786, 1724 (C═O stretching of phthalimide), 1658 (C═O stretching of PBI unit), 1377 (C−N stretching). ^{1}H NMR (DMSO-d_6, δ, ppm) of **PI−PBI1**: 8.13 (d, J = 7.8 Hz, ArH, 2H), 7.94 (d, J = 7.8 Hz, ArH, 2H), 7.79 (s, ArH, 2H), 7.36 (d, J = 9.0 Hz, ArH, 4H), 7.21 (d, J = 8.7 Hz, ArH, 2H), 7.15−7.08 (m, ArH, 6H), 2.30 (s, $ArCH_3$, 3H), 6.8−8.4 (bm, ArH of PBI containing unit, 0.23H (0.22H, calcd)). ^{1}H NMR (DMSO-d_6, δ, ppm) of **PI−PBI2.5**: 8.13 (d, J = 7.8 Hz, ArH, 2H), 7.94 (d, J = 7.8 Hz, ArH, 2H), 7.79 (s, ArH, 2H), 7.36 (d, J = 9.0 Hz, ArH, 4H), 7.21 (d, J = 8.7 Hz, ArH, 2H), 7.15−7.08 (m, ArH, 6H), 2.30 (s, $ArCH_3$, 3H), 6.8−8.4 (bm, ArH of PBI containing unit, 0.79H (0.56H, calcd)). ^{1}H NMR (DMSO-d_6, δ, ppm) of **PI−PBI5**: 8.13 (d, J = 7.8 Hz, ArH, 2H), 7.94 (d, J = 7.8 Hz, ArH, 2H), 7.79 (s, ArH, 2H), 7.36 (d, J = 9.0 Hz, ArH, 4H), 7.21 (d, J = 8.7 Hz, ArH, 2H), 7.15−7.08 (m, ArH, 6H), 2.30 (s, $ArCH_3$, 3H), 6.8−8.4 (bm, ArH of PBI containing unit, 1.3H (1.2H, calcd.)). ^{1}H NMR (DMSO-d_6, δ, ppm) of **PI−PBI10**: 8.13 (d, J = 7.8 Hz, ArH, 2H), 7.94 (d, J = 7.8 Hz, ArH, 2H), 7.79 (s, ArH, 2H), 7.36 (d, J = 9.0 Hz, ArH, 4H), 7.21 (d, J = 8.7 Hz, ArH, 2H), 7.15−7.08 (m, ArH, 6H), 2.30 (s, $ArCH_3$, 3H), 6.8−8.4 (bm, ArH of PBI containing unit, 2.5H (2.4H, calcd)). Anal. Calcd of **PI−PBI1**: C, 65.4; H, 3.02; N, 6.02. Found: C, 64.3; H, 3.37; N, 6.13. Anal. Calcd of **PI−PBI2.5**: C, 65.5; H, 3.01; N, 6.01. Found: C, 64.3; H, 3.36; N, 6.07. Anal. Calcd of **PI−PBI5**: C, 65.5; H, 2.99; N, 6.00. Found: C, 64.1; H, 3.58; N, 6.28. Anal. Calcd of **PI−PBI10**: C, 65.6; H, 2.95; N, 5.99. Found: C, 62.9; H, 3.34; N, 5.62.

General Measurement and Characterization. FT-IR spectra were measured by a Horiba FT-120 Fourier transform spectrophotometer. M_n and M_w values were evaluated by a Hitachi SEC with two polystyrene gel columns (Shodex GPC KD-804, KD-805). *N*,*N*-Dimethylformamide (DMF) containing 0.01 M LiBr was used as an eluent at a flow rate of 1.0 mL min^{-1} calibrated by polystyrene standard samples. Elemental analyses were performed on a Yanaco MT-6 CHN recorder elemental analysis instrument. Thermal properties were estimated from a Seiko TG/DTA 6300 thermal gravimetric analysis (TGA) system and a thermal analysis instrument of DSC-Q100 differential scanning calorimetry (DSC) under a nitrogen atmosphere at a heating rate of 10 and 6 °C/min, respectively. Electrochemistry was performed with a CHI 611B electrochemical analyzer. Cyclic voltammetry (CV) was performed by a three-electrode cell in which ITO (polymer film area about 0.7 × 0.5 cm^2) was used as a working electrode. A platinum wire was used as an auxiliary electrode. All cell potentials were taken with the use of a homemade Ag/AgCl, KCl(sat.) reference electrode. Absorption spectra were measured with a Hitachi U4100 UV−vis−NIR spectrophotometer. The thickness of the polymer film was measured with a Microfigure Measuring Instrument (Surfcorder ET3000, Kosaka Laboratory Ltd.). The morphologies of polymer film surface were obtained with a Nanoscope 3D Controller atomic force micrographs (AFM, Digital Instruments) operated in the tapping mode at room temperature.

Fabrication and Characterization of Memory Device. The indium tin oxide (ITO) glass substrates were cleaned stepwise by water, acetone, and isopropyl alcohol in an ultrasonic bath. The memory device was fabricated following the basic structures of ITO/PIs/Al. A well-dissolved polymer solution in DMAc was first filtered through 0.45 μm pore size of poly(tetrafluoroethylene) (PTFE) membrane syringe filter, spin-coated on top of an ITO glass substrate at a speed rate of 1000 rpm for 60 s, and then baked at 150 °C for 20 min in a nitrogen-filled glovebox. The thickness of the thin film was determined to be around 37−41 nm. The top electrode with a 300 nm of Al was deposited under vacuum through the shadow mask in a thermal evaporator. Each substrate contained the memory cells with a recorded area of 0.5 × 0.5 mm^2. The electrical characterization of the memory device was performed by a Keithley 4200-SCS semiconductor parameter analyzer equipped with a Keithley 4205-PG2 arbitrary waveform pulse generator. ITO was used as the cathode (maintained as common), and Al was set as the anode during the voltage sweep. All of the electronic measurements were performed in a glovebox.

Computational Methodology. All calculations were performed using the Gaussian 03 program package.[33] Optimized gas-phase ground states were calculated at the density functional theory (DFT) method, using the hybrid B3LYP exchange correlation functional and the split valence 6-31G(d) basic set (DFT//B3LYP/6-31G(d)).

RESULTS AND DISCUSSION

Synthesis and Characterization of CoPIs. The general synthetic strategy is shown in Scheme 1. The **PI−PBI0** was

synthesized by a two-step polycondensation of aromatic dianhydride (**6FDA**) with AMTPA, followed by chemical imidization using acetic anhydride and pyridine. On the other hand, the synthesis of other four coPIs (**PI−PBI1**, **PI−PBI2.5**, **PI−PBI5**, and **PI−PBI10**) was also carried out according to the similar procedure in *m*-cresol (which is known as a good solvent for perylene diimide system). The feeding ratios of **PBI** to **AMTPA** were set to be 1, 2.5, 5, and 10 mol %. The chemical imidization of all PAA was characterized by FT-IR spectra. All the PIs exhibited similar IR absorption peaks originated from the imide moieties located around 1780 cm^{-1} (ν_{as}, C═O), 1720 cm^{-1} (ν_s, C═O), and 1370 cm^{-1} (ν, C−N) as presented in Figure 1. The structures of all PIs were also

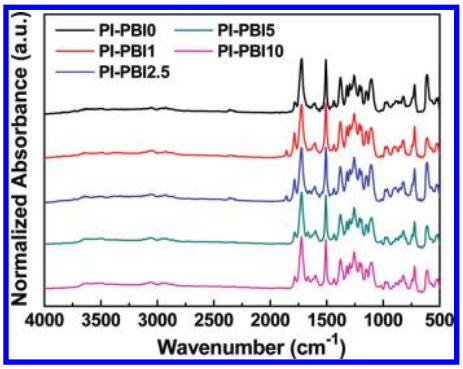

Figure 1. FTIR spectra of **PI−PBIX**.

characterized by ^{1}H NMR (Figure 2). The characteristic signals for perylene units of **PI−PBIX** were observed but very broadly in the range of 7.0−8.4 ppm. Thus, the structure determination and molar composition of **PBI** in **PI−PBIX** were performed by comparing the integral values of the whole ArH spectra (no. 1′−no. 7′ in Figure 2) with the $ArCH_3$ signal (no. 8 in Figure 2) of **AMTPA** unit. When the integral value of $ArCH_3$ signal was set to be 3, the observed integral values of ArH signals of **PI−PBI1**, **PI−PBI2.5**, **PI−PBI5**, and **PI−PBI10** were 18.2, 18.8, 19.3, and 20.5, respectively, which were consistent with those calculated values of 18.2, 18.6, 19.2, and 20.4, respectively. Also, the expected structures of all PIs were confirmed by elemental analysis. These results suggest that the molar ratios of **PBI** to **AMTPA** in **PI−PBIX** are close to the original relative feeding of monomers. In addition, all the polyimides showed high M_n from 18 to 42 kDa (Table 1) and were readily soluble in common organic solvents such as DMAc, dimethyl sulfoxide (DMSO), and *N*-methyl-2-pyrrolidone (NMP). However, further increase in the **PBI** content within the PIs makes **PI−PBIX** insoluble (for example, if **X** value is more than 10). The thermal properties of **PI−PBIX** were evaluated by TGA and DSC as summarized in Table 1. All the PIs possessed high thermal stabilities with a high decomposition temperature (T_d) at around 500 °C and glass transition temperature (T_g) not being observed below 300 °C (Figure S1 of Supporting Information). The excellent thermal properties of all the PIs are expected to meet the requirement of heat resistance in electronics industry.

Optical and Electrochemical Properties. The absorption spectra of the studied PIs were measured in the thin film (Figure 3), and the correlated optical parameters are listed in Table 1. All the copolyimides exhibit high energy absorption bands at 337 nm due to the localized $\pi-\pi^*$ transition from **AMTPA** segments, suggesting that five polyimides have similar conjugated length. However, one additional broad low energy optical absorption (peak at 497 and 544 nm) of **PI−PBI10** was observed, corresponding to the existence of **PBI** fragments and charge-transfer interaction between the electron-rich donors and electron-efficient acceptors. It also indicates that the acceptor strength of **PBI** is stronger than that of **6FDA** dianhydride. Optical band gaps were determined from

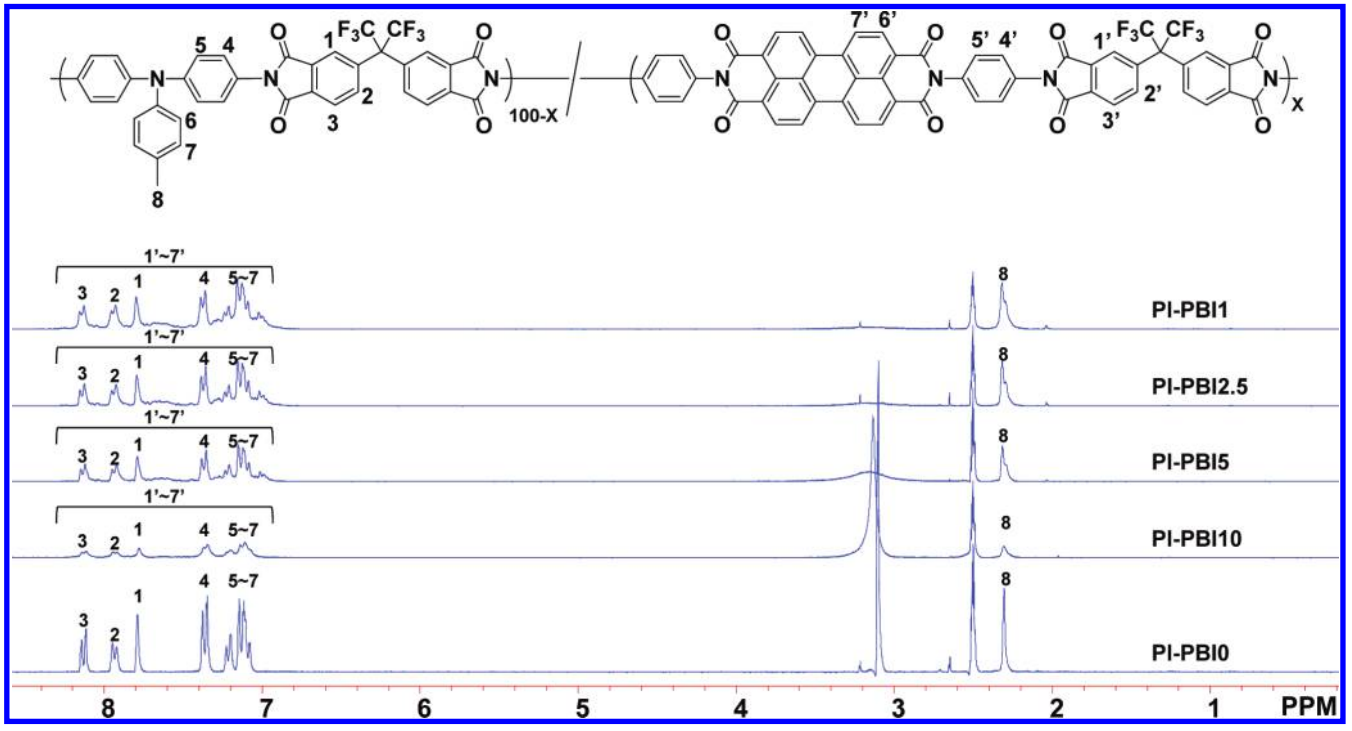

Figure 2. ^{1}H NMR spectra of **PI−PBIX** in DMSO-d_6.

dx.doi.org/10.1021/ma300732m | *Macromolecules* 2012, 45, 4556−4563

Table 1. Molecular Weights and Physical Properties of the Prepared Polyimides

polyimides	M_n (g/mol)[a]	M_w (g/mol)[a]	PDI[a]	T_d (°C)[b]	T_g (°C)[c]	band gap (eV)[d]	HOMO (eV)[e]	LUMO (eV)[e]
PI−PBI0	42 500	112 000	2.64	515	–	3.14	−5.31	−2.17
PI−PBI1	18 700	42 200	2.26	507	–	3.14	−5.31	−2.17
PI−PBI2.5	19 400	42 000	2.16	508	–	3.14	−5.31	−2.17
PI−PBI5	18 100	35 700	1.97	510	–	3.14	−5.31	−2.17
PI−PBI10	32 000	67 000	2.09	496	–	2.05	−5.22	−3.17

[a]Determined by SEC. [b]Determined by TGA. [c]Determined by DSC. The measurement was carried out in the range of 25−250 °C. [d]Estimated from the onset of absorption. [e]LUMO = HOMO + band gap.

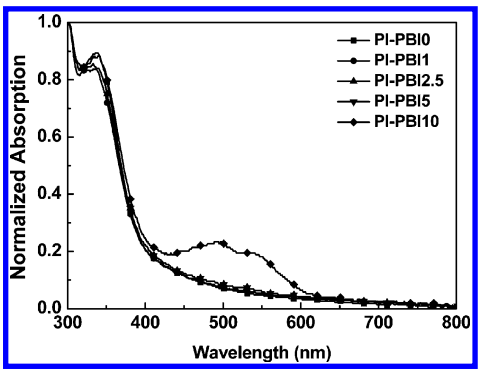

Figure 3. Optical absorption spectra of **PI−PBIX** thin film on quartz plate.

absorption edge to be 3.14 eV for **PI−PBI0**, **PI−PBI1**, **PI−PBI2.5**, and **PI−PBI5** and 2.05 eV for **PI−PBI10**. The smaller band gap for **PI−PBI10** relative to other PIs suggests that the band gap within **PI−PBIX** series can be red-shifted by increasing the **PBI** acceptor ability.

CV in dry acetonitrile with tetrabutylammonium hexafluorophosphate ($TPAPF_6$) as the supporting electrolyte under nitrogen flow was used to evaluate the oxidation characteristics. Figure 4 shows the result of CV traces. From these data, one

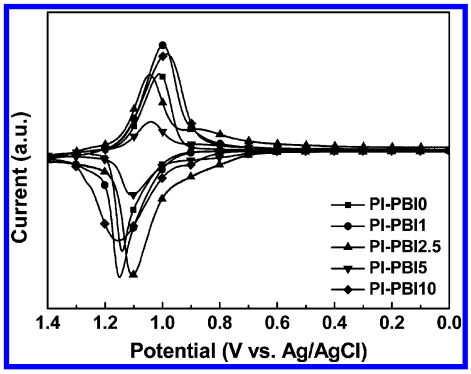

Figure 4. Cyclic voltammograms of **PI−PBIX**.

observes that all copolyimides exhibit quasi-reversible oxidation waves which are reasonably attributed to the presence of the TPA fragments. The highest occupied molecular orbital (HOMO) energy levels of the PIs were calculated from the onset of oxidation waves in CV with reference to ferrocence (4.8 eV) by the following equation: HOMO = $-(E^{onset} + 4.8 - E_{ferrocene})$. Besides, the lowest unoccupied molecular orbital (LUMO) energy levels were estimated from the difference between the optical band gap and HOMO level. Relevant data are demonstrated in Table 1. No significant differences were observed in either HOMO or LUMO level except for the **PI−PBI10**. As noticed, increasing the strong electron-withdrawing of **PBI** repeat units until 10 mol % increases the energy of HOMO by 0.09 eV and lowers the energy of LUMO by 1 eV, readily accommodated by the intra- or intermolecular charge transfer between **AMTPA** donors and **PBI** acceptors with enhanced electron delocalization across the backbone. Overall, the optical and CV results indicate that the energy levels of frontier orbital can be tailored by the loading ratio on the electron affinity of the **PBI** units.

Memory Characteristics. The effects of relative **AMTPA**/**PBI** composition in imide-based random coPIs on memory device performance were systematically investigated. The memory devices of coPIs were fabricated on the basis of ITO/PIs/Al three-layer sandwiched device configuration, and the performance was tested by the current−voltage (I−V) characteristics under the inert atmosphere. ITO was used as the anode, and Al was set as the cathode (maintained as common) in all electrical measurements. Representative I−V curves for memory device based on **PI−PBI0** (in steps of 0.1 V) are shown in Figure 5. Starting with low-conductivity OFF state of

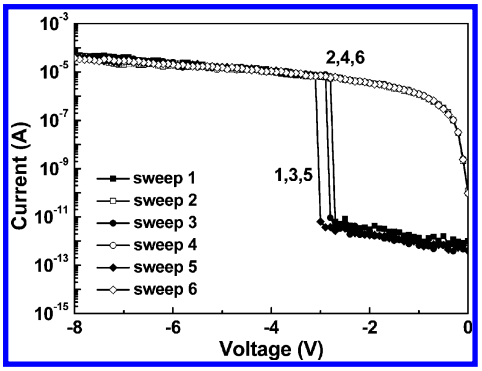

Figure 5. Current−voltage (I−V) characteristics of **PI−PBI0** memory device.

as-fabricated device, the current increases slowly in the range of 10^{-13}−10^{-11} A with the applied negative voltage. The current remains low until the threshold voltage of about −2.8 V. When the voltage increases further, the current increases abruptly from 10^{-11} to 10^{-5} A (sweep 1), thus indicating electronic transition to high-conductivity ON state that can serve as the "writing" process. A distinct hysteresis can be seen in the bistable **PI−PBI0** device with an ON/OFF current ratio up to 10^6. The ON state can be kept during a subsequent sweep from 0 to −8 V (sweep 2). After reading the ON state in the negative sweep and turning off the power for about 4 min, the device can be conducted to reprogram from OFF state to ON state again with a negative biased sweep (sweep 3) and remains in the ON state (sweep 4). The **PI−PBI0** memory device exhibits repeated operation from the sweep 5 and sweep 6, and the ON state could not be maintained after the removal of power

dx.doi.org/10.1021/ma300732m | Macromolecules 2012, 45, 4556−4563

and would gradually relax back to the OFF state. The electrical switching behavior concludes that the **PI−PBI0** memory device exhibits the volatile nature because the stored data are finally lost. Also, for the case of higher PBI loading in **PI−PBIX** polymers (for **X** = 1 and 2.5), similar volatile nature can be repeated at several sweeps in the same cell or different devices with reproducible data (Figures S2 and S3 of Supporting Information). The OFF state can be further recovered to a stored state again with a small variation on reapplied switching voltage bias. The long-term and stimulus stability of the memory effect was also evaluated under the same condition. Figure 6 shows the retention times and stress tests of both the

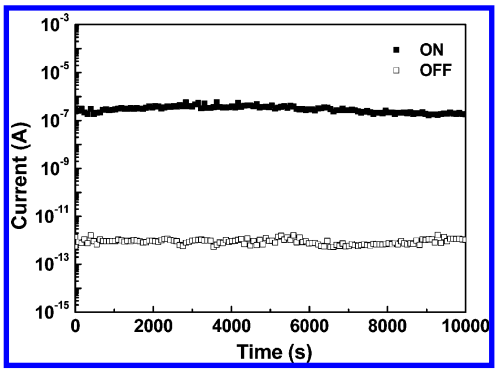

Figure 6. Retention times on the ON and OFF states of the **PI−PBI2.5** device under a continuous readout voltage.

ON and OFF states of the **PI−PBI2.5** device. Initially, the memory device switches to a high conductivity state. The ON state can be maintained without obvious degradation for at least 10^4 s under a constant stress of −1 V. Then, the device is set back to the OFF state, it can also be persisted for the whole readout test period, and the ON/OFF current ratio is kept around 10^6. Figure 7 shows cycles of a pulse voltage stress with a pulse width of 1 μs without significant change in ON state and OFF state current for at least 10^8 continuous read pulses of −1 V.

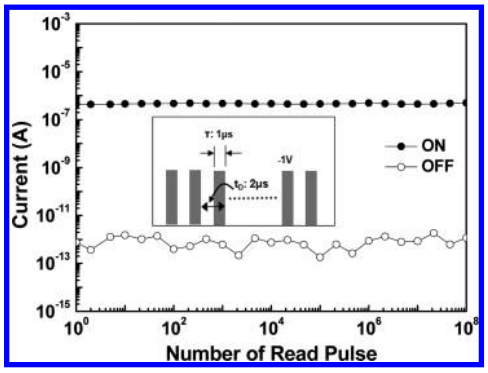

Figure 7. Stimulus effect of read pulses on the ON and OFF states of the **PI−PBI2.5** device. The inset shows the pulse shapes in the measurement.

Further increasing fraction in the **PBI** moieties, **PI−PBI5** exhibits the typical WORM memory effect. The devices based on **PI−PBI5** were scanned through five voltage sequences: 0 to −8.0 V (for sweep 1 to 4) and 0 to 8.0 V (sweep 5) in steps of 0.1 V, as shown in Figure 8. Initially, this device is in the OFF state, the current increases rapidly 6 orders of magnitude at

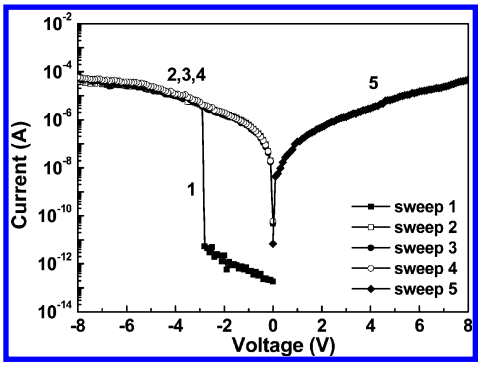

Figure 8. Current−voltage (I−V) characteristics of the **PI−PBI5** memory device.

−2.9 V, and it changes to the ON state. The device cannot return to the OFF state even after removing the power supply (sweep 2) or applying the same magnitude reverse voltage (sweep 5). The ON state can be retained permanently in the subsequent voltage sweeps (sweeps 3 and 4). The **PI−PBI5** thin film sandwiched between ITO and Al electrodes exhibits single resistive switch. The **PI−PBI10** device with more **PBI** units also shows the irreversible WORM memory performance, as shown in Figure S4 of the Supporting Information. A remarkable current hysteresis was observed at one-direction resistive switching from OFF to ON state.

Mechanism of Polyimides Memory Devices. To gain insight into the switching mechanism of memory device based on **PI−PBIX** active layer, the electronic properties were studied by DFT and I−V characteristics of both ON and OFF state were analyzed. Calculations of the optimized geometry and molecular orbitals of the basic unit (BU) were carried out at the B3LYP/6-31G(d) level with the Gaussian 03 program package. The mechanism of **PI−PBI0** of electronic transition can be explained from electric field induced charge transfer between the **AMTPA** donor and **6FDA** acceptor.[10−13,17−20] Similar molecular simulation of the BU of **PI−PBI0** was demonstrated (Figure S5 of Supporting Information) relative to the **TP6F−PI** (without methyl group attached on the triphenylamine) proposed by Kang's group.[10] The relative ordering of the occupied and virtual molecular orbitals give a reasonable indication of the excited properties (from overlapping of the HOMO and LUMO+2) and charge transport ability. The HOMO and LUMO+2 orbitals are localized at the donor while LUMO and LUMO+1 orbitals are located at acceptor which implies that CT can occur to form conductive channel through the process either indirectly from the LUMO+2 of donor to the LUMO+1 and then to the LUMO of acceptor or directly from the HOMO of donor to the LUMO of acceptor.[10] The unstable CT state contributes to the charge recombination, and the device rapidly returns to the original OFF state due to the limited delocalization of **AMTPA** moieties and low theoretical dipole moment of basic repetitive unit of **PI−PBI0**.

The **PBI/AMTPA** composition effect of memory performance was investigated as a molar ratio of **PBI** moieties in the **PI−PBIX** random coPIs. **PI−PBI1** and **PI−PBI2.5** devices still maintain the volatile behavior since unstable charge transfer through the presence of donor and acceptor forms a charge-separated state in a compound inferred from the locations of frontier orbitals and change in the distribution of electron density upon excitation. However, **PI−PBI5** and **PI−PBI10** devices were determined to be nonvolatile WORM memories

dx.doi.org/10.1021/ma300732m | *Macromolecules* 2012, 45, 4556−4563

as explained above. The differences in the structural variations from the **PBI** molar ratio play an important role for governing the recording reversibility. The CT state mediated by the donor and acceptor located in the polymer backbone is responsible for all the resistive switching. The stability of conductive CT complexes may depend on the recombination abilities of the generated holes and electrons possibly referred to the donor−acceptor strength. Theoretical modeling was used to calculate the electronic properties to confirm the **AMTPA**, **6FDA**, and **PBI** moieties. The higher HOMO energy level of **AMTPA** (−4.87 eV) indeed indicates that it functions as the hole accepting unit, while the lowest LUMO of **PBI** (−3.40 eV) relative to **6FDA** (−2.69 eV) indicates the strongest electron-withdrawing ability of **PBI** that is enriched with electrons. Once a high conductivity path is formed in the **PI−PBI5** or **PI−PBI10** device, charged carriers can be retained due to stable charge-transfer complex from the increasing amounts of incorporation on the strong **PBI** acceptors, resulting in the significant increase in the polarity of **PI−PBI5** or **PI−PBI10**. Besides, the capable charge trapping environment may be established from the deepest LUMO energy level of **PBI** units which increase the back-charge-transfer energy barrier and possibly help to prevent recombination of segregated charges even through applying the high negative and positive voltage.

Figure 9 shows the *I*−*V* curves of **PI−PBI5** device for OFF state, and the conduction state has well been characterized by

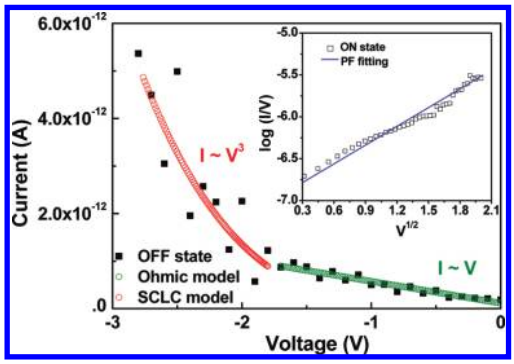

Figure 9. Experimental and fitted current−voltage (*I*−*V*) characteristics of the **PI−PBI5** memory device in the OFF and ON states.

ohmic conduction relationship ($I \sim V$) and trap-limited space-charge-limited current (SCLC; $I \sim V^{m+1}$ ($m > 1$))[15,34] in the range of 0 to −1.7 V and −1.7 to −2.8 V, respectively, indicating that the carriers overcome the energy barrier and flow through the device by Ohmic conduction and trap-free SCLC process sequentially at the higher bias. The power-law region indicates that the switching is triggered by carrier injection and hopping processes between the PIs chains. When the applied voltage exceeds the threshold value, the numerous generated charges and charge-transfer process rapidly yield a conducting path. As shown in inset of Figure 9, the obtained slope in a plot of $\log(I/V)$ vs $V^{1/2}$ of ON state is nearly equal to one. It indicates that the Poole−Frenkel emission is dominant in the ON state, reflecting the change in the conducting process at this stage.[35]

The **6FDA/AMTPA** moieties positioned in the main chain of **PI−PBI0** make the charge-transfer state easily be neutralized after removal of the applied voltage. Therefore, controlling the relative **PBI/AMTPA** ratio in **PI−PBIX** copolymers system can be effectively operated between the volatile to nonvolatile transition in terms of the balance on donor−acceptor charge-transfer interaction and trapping condition under an electric field.

CONCLUSIONS

We have successfully designed and synthesized a series of **PBI/AMTPA** random coPIs, **PI−PBIX** (**X = 0**, **1**, **2.5**, **5**, **10**), where **6FDA** is covalently attached with adjacent **PBI** or **AMTPA** groups in a random arrangement. The electron-donating **AMTPA** and electron-withdrawing **PBI** were copolymerized with **6FDA** by chemical imidization. The loading molar composition of **PBI** in **PI−PBIX** copolymers can be used to modulate the optical and electronic properties by intramolecular charge transfer. The memory devices with a configuration of ITO/**PI−PBIX**/Al exhibited distinct switching characteristics which were found to be varied continuously with copolymer composition. The (**PBI-0**, **PBI-1**, **PBI-2.5**) and (**PBI-5**, **PBI-10**) devices provided volatile and nonvolatile WORM behavior, respectively. The theoretical simulation suggested that the charge-transfer mechanism could be used to explain the memory behavior and more stable charge-transfer complex and charge trapping condition with a higher **PBI** content for obtaining WORM memory characteristics. Specifically, the importance of these results provided that random coPIs with multiple relative donor/acceptor ratios in the main chain represent the design concept for a new class of PIs with readily tunable electronic memory performance.

ASSOCIATED CONTENT

Supporting Information

TGA curves of **PI−PBIX** random copolymers; *I*−*V* characteristics of **PI−PBI1**, **PI−PBI2.5**, and **PI−PBI10** memory devices; theoretical calculation on geometries and electronic structures of basic units of **PI−PBI0**. This material is available free of charge via the Internet at http://pubs.acs.org.

AUTHOR INFORMATION

Corresponding Author

*E-mail: chenwc@ntu.edu.tw (W.-C.C.); ueda.m.ad@m.titech.ac.jp (M.U.); clliu@yz.yamagata-u.ac.jp (C.-L.L.).

Present Address

[#]Department of Chemical and Materials Engineering, National Central University Taoyuan 32001, Taiwan.

Author Contributions

[⊥]T. Kurosawa and Y.-C. Lai equally contributed to this work.

Notes

The authors declare no competing financial interest.

ACKNOWLEDGMENTS

T.K. is thankful for support from the Japan Society for the Promotion of Science (23·2900). The authors acknowledge final support from the National Science Council of Taiwan, the Excellence Research Program of National Taiwan University, and Dissemination of Tenure Tracking System Program of Ministry of Education, Culture, Sports, Science and Technology−Japan. The helpful discussion and kindly instrumental support from Prof. J. Kido and Prof. Z. Hong of Yamagata University are highly appreciated.

REFERENCES

(1) Waser, W.; Aono, M. *Nat. Mater.* **2007**, *6*, 833.
(2) Sawa, A. *Mater. Today* **2008**, *11*, 28.

(3) Ling, Q. D.; Liaw, D. J.; Zhu, C.; Chan, D. S. H.; Kang, E. T.; Neoh, K. G. *Prog. Polym. Sci.* **2008**, *33*, 917.
(4) Ling, Q. D.; Liaw, D. J.; Teo, E. Y. H.; Zhu, C.; Chan, D. S. H.; Kang, E. T.; Neoh, K. G. *Polymer* **2007**, *48*, 5182.
(5) Yang, Y.; Ouyang, J.; Ma, L.; Tseng, R. J. H.; Chu, C. W.; Yang, Y. *Adv. Funct. Mater.* **2007**, *19*, 1452.
(6) Heremans, P.; Gelinck, G. H.; Muller, R. M.; Baeg, K. J.; Kim, D. Y.; Noh, Y. Y. *Chem. Mater.* **2011**, *23*, 341.
(7) Cho, B.; Song, S.; Ji, Y.; Kim, T. W.; Lee, T. *Adv. Funct. Mater.* **2011**, *21*, 2806.
(8) Liu, C. L.; Chen, W. C. *Polym. Chem.* **2011**, *2*, 2196.
(9) Lee, S. J. *J. Mater. Chem.* **2011**, *22*, 14097.
(10) Ling, Q. D.; Chang, F. C.; Song, Y.; Zhu, C. X.; Liaw, D. J.; Chan, D. S. H.; Kang, E. T.; Neoh, K. G. *J. Am. Chem. Soc.* **2006**, *128*, 8732.
(11) Liu, Y. L.; Ling, Q. D.; Kang, E. T.; Neoh, K. G.; Liaw, D. J.; Wang, K. L.; Liou, W. T.; Zhu, C. X.; Chan, D. S. H. *J. Appl. Phys.* **2009**, *105*, 044501.
(12) Wang, K. L.; Liu, Y. L.; Lee., J. W.; Neoh, K. G.; Kang, E. T. *Macromolecules* **2010**, *43*, 7159.
(13) Wang, K. L.; Liu, Y. L.; Shih, I. H.; Neoh, K. G.; Kang, E. T. *J. Polym. Sci., Polym. Chem.* **2010**, *48*, 5790.
(14) Lee, T. J.; Chang, C. W.; Hahm, S. G.; Kim, K.; Park, S.; Kim, D. M.; Kim, J.; Kwon, W. S.; Liou, G. S.; Ree, M. *Nanotechnology* **2009**, *20*, 135204.
(15) Kim, K.; Park, S.; Hahm, S. G.; Lee, T. J.; Kim, D. M.; Kim, J. C.; Kwon, W.; Ko, Y. G.; Ree, M. *J. Phys. Chem. B* **2009**, *113*, 9143.
(16) Kim, D. M.; Park, S.; Lee, T. J.; Hahm, S. G.; Kim, K.; Kim, J. C.; Kwon, W.; Ree, M. *Langmuir* **2009**, *25*, 11713.
(17) Kuorosawa, T.; Chueh, C. C.; Liu, C. L.; Higashihara, T.; Ueda, M.; Chen, W. C. *Macromolecules* **2009**, *42*, 4456.
(18) You, N. H.; Chueh, C. C.; Liu, C. L.; Ueda, M.; Chen, W. C. *Macromolecules* **2009**, *42*, 4456.
(19) Liu, C. L.; Kurosawa, T.; Yu, A. D.; Higashihara, T.; Ueda, M.; Chen, W. C. *J. Phys. Chem. C* **2011**, *115*, 5930.
(20) Tian, G.; Qi, S.; Chen, F.; Shi, L.; Hu, W.; Wu, D. *Appl. Phys. Lett.* **2011**, *98*, 203302.
(21) Zhuang, X. D.; Chen, Y.; Li, B. X.; Ma, D. G.; Zhang, B.; Li, Y. *Chem. Mater.* **2010**, *22*, 4455.
(22) Fang, Y. K.; Liu, C. L.; Li, C.; Lin, C. J.; Mezzenga, R.; Chen, W. C. *Adv. Funct. Mater.* **2010**, *20*, 3012.
(23) Fang, Y. K.; Liu, C. L.; Chen, W. C. *J. Mater Chem.* **2011**, *21*, 4778.
(24) Fang, Y. K.; Liu, C. L.; Yang, G. Y.; Chen, P. C.; Chen, W. C. *Macromolecules* **2011**, *44*, 2604.
(25) Kang, N. G.; Cho, B.; Kang, B. G.; Song, S.; Lee, T.; Lee, J. S. *Adv. Mater.* **2012**, *24*, 385.
(26) Tseng, R. J.; Huang, J.; Ouyang, J.; Kaner, R. B.; Yang, Y. *Nano Lett.* **2005**, *5*, 1077.
(27) Ouyang, J.; Chu, C. W.; Szmanda, C. R.; Ma, L.; Yang, Y. *Nat. Mater.* **2004**, *3*, 918.
(28) Chen, J. S.; Liu, C. L.; Sun, Y. S.; Tung, S. H.; Chen, W. C. *Soft Matter* **2012**, *8*, 526.
(29) Liu, G.; Ling, Q. D.; Teo, E. Y. H.; Zhu, C. X.; Chan, D. S. H.; Neoh, K. G.; Kang, E. T. *ACS Nano* **2009**, *3*, 1929.
(30) Zhang, X. D.; Chen, Y.; Liu, G.; Li, P. P.; Zhu, C. X.; Kang, E. T.; Neoh, K. G.; Zhang, B.; Zhu, J. H.; Li, Y. X. *Adv. Mater.* **2010**, *22*, 1731.
(31) Yu, A. D.; Liu, C. L.; Chen, W. C. *Chem. Commun.* **2012**, *48*, 383.
(32) Neuber, C.; Bäte, M.; Giesa, R.; Schmidt, H. W. *J. Mater. Chem.* **2006**, *16*, 3466.
(33) *Gaussian 03, Revision B.04*; Gaussian, Inc.: Wallingford, CT, 2004.
(34) Shang, D. S.; Wang, Q.; Chen, L. D.; Dong, R.; Li, X. M.; Zhang, W. Q. *Phys. Rev. B* **2006**, *73*, 245427.
(35) Sze, S. M. *Physics of Semiconductor Devices*; Wiley: New York, 1998.
(36) Zhan, X.; Facchetti, A.; Barlow, S.; Marks, T. J.; Ratner, M. A.; Wasielewski, M. R.; Marder, S. R. *Adv. Mater.* **2011**, *23*, 268.
(37) Neuteboom, E. E.; Meskers, S. C. J.; van Hal, P. A.; van Duren, J. K. J.; Meijer, E. W.; Janssen, R. A. J.; Dupin, H.; Pourtois, G.; Cornil, J.; Lazzaroni, R.; Bredas, J. L.; Beljonne, D. *J. Am. Chem. Soc.* **2003**, *125*, 8625.
(38) Van der Boom, T.; Hayes, R. T.; Zhao, Y.; Bushard, P. J.; Weiss, E. A.; Wasielewski, M. R. *J. Am. Chem. Soc.* **2002**, *124*, 9582.